Title

Three-Dimensional Crystals Assembled by Linear Oligopeptoids

Journal

Nano Letters, 25(31)

ISSN

1530-6984

Authors

Lee, Yen Jea

Ercius, Peter

Luo, Xubo

et al.

Publication Date

2025-08-06

DOI

10.1021/acs.nanolett.5c02506

Peer reviewed

NANO LETTERS

pubs.acs.org/NanoLett

Letter

Three-Dimensional Crystals Assembled by Linear Oligopeptoids

Yen Jea Lee, Peter Ercius, Xubo Luo, Glenn L. Butterfoss, Tianyi Yu, Jian Zhang, David Prendergast, Andrew M. Minor, Nitash P. Balsara, Ronald N. Zuckermann,* Brooks A. Abel,* and Xi Jiang*

Cite This: *Nano Lett.* 2025, 25, 11940−11946

Read Online

ACCESS | Metrics & More | Article Recommendations | Supporting Information

ABSTRACT: The rational construction of three-dimensional (3D) crystalline lattices from synthetic short-chain polymers remains a significant challenge due to the lack of inherent driving forces to enable crystal growth in all three dimensions. Here, we report the design of 3D peptoid crystals from linear peptoid hexamers, derived from amphiphilic diblock sequences that typically form crystalline two-dimensional (2D) nanosheets. By removing the amorphous domains and tuning the chain termini, crystalline lamellae up to 500 nm thick were achieved, far exceeding the thickness of typical nanosheets (on the order of a few nanometers). These 3D crystals form via the stacking of unit cells with lattice parameters similar to those in 2D nanosheets, where terminal groups, particularly compact C-terminal moieties, facilitate vertical growth and enhance crystallinity. This study highlights the importance of atomic precision in terminus chemistry for achieving long-range ordering and isotropic crystal growth in the design of macroscale crystals from oligomeric peptoids.

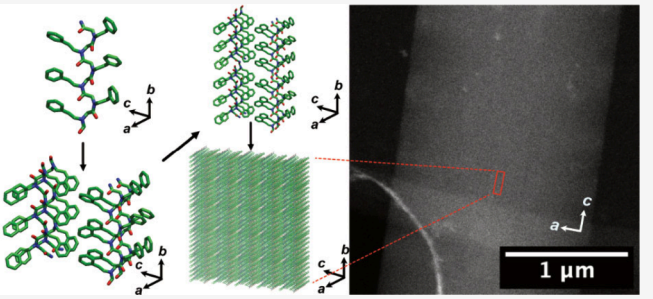

KEYWORDS: *peptoid, 3D crystal, 4D-STEM, self-assembly, terminus*

Crystallinity of organic materials, which varies greatly across chemical structures from small molecules to large polymers, plays a crucial role in nanomaterial performance but differs significantly between polymer crystals and small molecule crystals in terms of tunability and structural heterogeneity.[1−3] In-between these extremes are oligomeric materials,[4] like peptides[5−7] and biomimetic polymers,[8,9] where they have demonstrated importance to molecular separation,[10] drug delivery,[11,12] and energy conversion.[13] However, it remains a challenge to rationally design their three-dimensional (3D) crystal lattices, due to their many degrees of freedom and multitude of intra- and intermolecular interactions.[11,14−19]

Sequence-defined oligomers provide an ideal platform to study the impact of increasing chain length on crystallization. As an oligomeric chain grows, it gradually moves from being small-molecule like to polymer-like, and the increasing degree of conformational heterogeneity poses both a challenge to control, as well as to characterize using conventional tools.[20] Peptoids[21] offer atomic-scale precision in designing properties to explore the crystallization behavior of sequence-defined oligomers. The development of 3D crystals from oligopeptoids is critical to create complex architectures with tailored properties for emerging requirements in energy storage, molecular separation, and catalysis. This can be achieved by atomic-level tailoring of the peptoid chemical structure, which offer an unprecedented advantage over conventional 3D crystals.

Amphiphilic diblock peptoids can self-assemble into well-ordered two-dimensional (2D) nanostructures with crystalline hydrophobic cores and amorphous hydrophilic shells.[22−24] The crystalline cores of amphiphilic diblock peptoids comprise hydrophobic blocks (≥6 monomers) with unhindered side chains. However, translating 2D nanoscale order into 3D crystallinity is challenging, especially for chain lengths longer than six monomers that lack structure-inducing side chains, despite >100 high-resolution peptoid structures being reported.[25] The formation of 3D crystals from linear hexameric oligopeptoids remains an open question.

Herein, we studied three hexameric oligopeptoids with distinct terminal groups: formylhexakis[*N*-(2-phenethyl)-glycine] ($FNpe_6$), which has a formylated N-terminus and an unmodified C-terminal carboxamide (Figure 1A), formylpentakis[*N*-(2-phenethyl)glycine]-*N*-methyl-*N*-2-phenethylcarboxamide ($FNpe_5Nmepe$) featuring a more compact C-terminus (Figure 1B), and formylpentakis[*N*-(2-phenethyl)-glycine]phenethyl ester ($FNpe_5OPe$) with an even smaller ester end group (Figures S1−S4 and Table S1).

These oligopeptoids reside within the structurally flexible chain-like oligomeric regime, where crystallization behavior is challenging. This regime bridges the gap between small organic molecules and conventional polymers. We reasoned that

Received: May 7, 2025
Revised: July 23, 2025
Accepted: July 24, 2025
Published: July 28, 2025

https://doi.org/10.1021/acs.nanolett.5c02506
Nano Lett. 2025, 25, 11940−11946

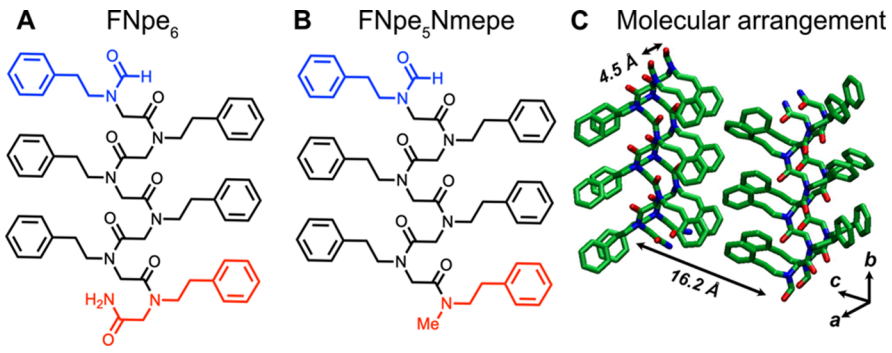

Figure 1. Chemical structures of oligomeric peptoids (A) $FNpe_6$ and (B) $FNpe_5Nmepe$, with the same C-termini highlighted in blue and the different N-termini in red. (C) Universal molecular arrangement of 2D nanosheets formed by a hydrophobic block identical to $FNpe_6$ without the C-terminus, as previously observed in amphiphilic diblock peptoids.[23] The configuration includes four molecules vertically aligned in two rows. The *a* direction corresponds to the alignment of molecules within rows, while the *c* direction indicates the spacing between rows, and the *b* direction runs parallel to the molecules. The electron beam used in imaging these 2D nanosheets is perpendicular to the *ac* plane. The *a* spacing is the distance between molecules within a row, and the *c* spacing is the distance between rows.

terminal group modifications in oligopeptoids, which are exposed and present at intermolecular lattice interfaces, can direct 3D crystallization by facilitating out-of-plane vertical growth, even in structurally flexible regimes. 3D crystals with thicknesses up to hundreds of nanometers were obtained by dissolving oligopeptoids in a heated mixed solvent of dimethylformamide (DMF) and water, followed by slow cooling. Structural analyses using cryogenic transmission electron microscopy (cryo-TEM), microelectron diffraction (microED), four-dimensional scanning transmission electron microscopy (4D-STEM), atomic force microscopy (AFM), and X-ray diffraction (XRD) showed that these 3D crystals retain the similar unit cell observed in previous 2D nanosheets with diblock peptoids (Figure 1C), where the vertical growth was blocked due to the presence of amorphous hydrophilic blocks.[23,26−30] Changes in the thickness and melting temperature reflect crystallinity differences driven by terminal group identity. Virtual bright-field imaging from 4D-STEM revealed spatial heterogeneity in crystallinity, demonstrating that termini design governs the length scale of molecular ordering. Our study demonstrates the successful formation of 3D crystals from linear oligopeptoids and provides insights into the role of terminal group modifications in controlling 3D crystal growth.

The AFM height image in Figure 2A shows that the 3D crystals formed by $FNpe_6$ are needle-shaped, with lengths of over 10 μm (Figure S5). A thickness distribution was measured from over 100 crystals (Figure S6), and the number-averaged thickness (H_n) was found to be 43 nm and weight-averaged thickness H_w at 52 nm (Figure 2B).

The XRD pattern in Figure 2C reveals key structural features of the lattice (Figure S7). A major peak appears at 16.05 Å, which is attributed to the (02) reflection, corresponding to the distance between two rows of peptoids along the *c* direction (Figure 1C). Due to symmetry, the actual lattice spacing (01) along the *c* direction is 32.1 Å, consistent with the observed *Cm* plane group in 2D nanosheets.[23,32] The presence of forbidden symmetry where $h+k$ is odd, such as (10), (01), (12), and (23), supports the interpretation that the 5.36 Å peak is the sixth-order reflection (06) of the 32.1 Å spacing (01). The 4.51 Å spacing (10) corresponds to the distance between vertically aligned peptoid molecules in a row (*a* spacing). A weak, broad peak at 4.77 Å and a strong peak at 4.19 Å are also observed. The Miller indices of these two peaks remain unclear because they have not been observed in previous characterizations of diblock peptoid nanosheets.[26,27,29,33−38] Overall, the XRD data confirm that the 3D crystals retain a unit cell arrangement analogous to that of the 2D nanosheets, but with more high-order reflections due to the increased thickness.[26]

Figure 2D shows a $FNpe_5Nmepe$ crystal with a length of over 20 μm. In contrast to $FNpe_6$ crystals, thickness measurements from over 100 $FNpe_5Nmepe$ crystals revealed a significantly greater H_n of 484 nm and H_w at 677 nm (Figure 2E). The XRD profile in Figure 2F displays several notable spacings, including 5.40 Å (06) and 4.57 Å (10), as well as 16.21 Å (02). The presence of additional peaks at 5.79, 5.16, 4.83, and 4.36 Å suggests a higher crystallinity in $FNpe_5Nmepe$ crystals. This is likely due to a more ordered molecular arrangement along the vertical direction (*b* direction), facilitated by the short methyl group at the *C*-terminus. Notably, some peaks of $FNpe_5Nmepe$ crystals exhibit a consistent 0.6 Å shift compared to those of $FNpe_6$ crystals. Specifically, the peak at 4.19 Å in $FNpe_6$ crystals shifts to 4.25 Å in $FNpe_5Nmepe$ crystals, while the peaks at 4.51 and 4.77 Å in $FNpe_6$ crystals shift to 4.57 and 4.83 Å, respectively, in $FNpe_5Nmepe$ crystals (comparing Figure 2C to Figure 2F). These shifts indicate subtle changes in the unit cell dimensions between the two systems.

A summary of structural characteristics of 3D crystals is shown in Figure 2G. The unit cell dimensions in 3D crystals are comparable to those of 2D nanosheets formed from the amphiphilic diblock peptoids with same hydrophobic block as $FNpe_6$. However, the melting temperature increases significantly from 93 °C in 2D nanosheets to 148 °C in 3D crystals formed by $FNpe_6$ where the crystalline core is formed by the same peptoid blocks.[39] The melting temperature further increased to 172 °C in crystals formed by $FNpe_5Nmepe$ (Figure S8). The enthalpy change (ΔH) suggests that $FNpe_5Nmepe$ crystals exhibit higher crystallinity which agrees with the XRD results.

The lattice structures cannot be directly solved using X-ray crystallography due to the isotropic dimensions of the crystals, which have thicknesses of hundreds of nanometers. The direct atomic-scale cryo-TEM imaging is not feasible due to the thickness of 3D crystals compared to the monolayer 2D nanosheets. Nevertheless, the power spectrum of the cryo-TEM image exhibits the featured spacings at 4.6 Å (10) and 16.1 Å (02) (Figure S9). MicroED was also carried out for the ab initio resolve of the lattice structure.[40] However, the appearance of split and arc-shaped spots at high tilt angles hinders the indexing

https://doi.org/10.1021/acs.nanolett.5c02506
Nano Lett. 2025, 25, 11940−11946

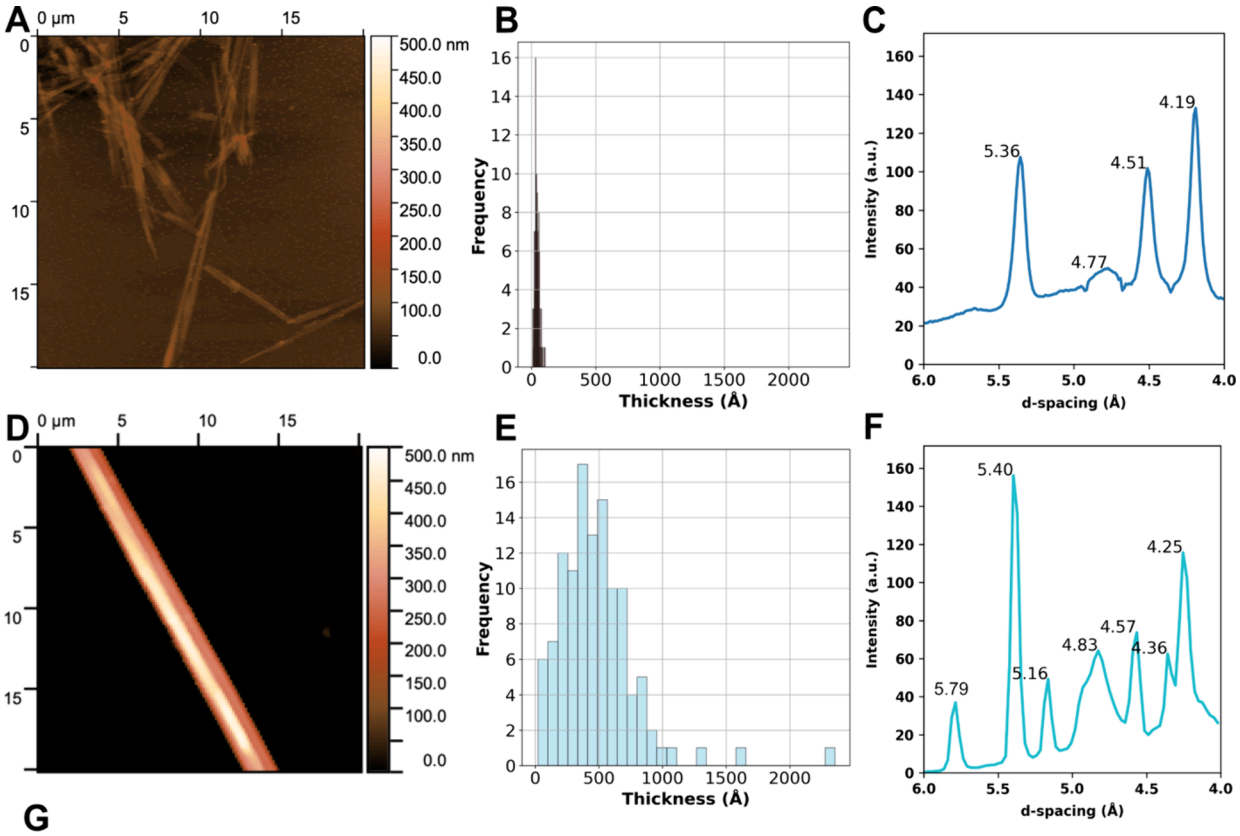

G

Polypeptoids	Solutions	Morphology	(10) (Å)	(01) (Å)	Tm (°C)	ΔH (kcal/mol)
Nte_4Npe_6[#]	THF/H_2O	2D nanosheets	4.5	16.2	93	not measured
$FNpe_6$	DMF/H_2O	3D crystal	4.5	32.2	148	7.4
$FNpe_5Nmepe$	DMF/H_2O	3D crystal	4.6	32.4	172	13.2

Figure 2. (A) AFM height image of 3D crystals formed by $FNpe_6$. (B) Histogram of AFM height profiles of over 100 3D crystals. (C) High spatial frequency section of the XRD profile obtained from 3D crystals formed by $FNpe_6$. The spacings of major peaks are labeled. (D–F) ues of parts A–C, obtained from the 3D crystals formed by $FNpe_5Nmepe$. (G) Summary of characteristics of 3D crystals. All *d* spacings are rounded to one decimal place for consistency. More optical microscopy micrographs, AMF images, DSC measurements, and the full XRD profiles are shown in Supporting Information. [#]The 2D nanosheet, which was formed by a hydrophobic block in amphiphilic diblock peptoids identical to $FNpe_6$ without the change to the *C*-terminus in the previous study.[23] The thickness of 3D crystals was calculated in number-averaged thickness (H_n) and weight-averaged thickness (H_w). The formulas are defined as $H_n = [\sum(N_iH_i)]/\sum N_i$ and $H_w = [\sum(N_iH_i^2)]/\sum(N_iH_i)]$, where H_i represents the height of the individual crystals and N_i is the number of crystals that have height H_i.[31]

and scaling in crystallography (Figure S10). This suggests that these 3D crystals are not isotopically homogeneous.

4D-STEM, a technique that utilizes an electron probe to scan the crystal, was employed to elucidate the local heterogeneity within 3D peptoid crystals.[41] This approach allows for the acquisition of electron diffraction patterns at precise scanning locations, providing detailed structural information that reveals variations within the crystal structure, unlike the global information obtained from conventional diffraction methods. It has been successfully used to resolve the local crystallinity in polymer thin films and organic semiconductors.[42−45]

A high-angle annular dark field scanning transmission electron microscopy (HAADF-STEM) micrograph of a crystal formed by $FNpe_6$ is presented in Figure 3A, which has two areas marked by colored boxes 1 and 2. The electron diffraction patterns from these areas, illustrated in Figure 3B,C, confirm the presence of similar unit cell dimensions previously described in Figure 1C, with spacings along the *c* and *a* directions of 16.1 and 4.5 Å, respectively. First-order diffraction spots (01) at 32.2 Å and (10) at 4.5 Å, which represent the true *c* and *a* lattice spacings, are absent due to constraints in the *Cm* plane symmetry; such spots are forbidden when the sum of the Miller indices *h* and *k* is odd in (*hk*) reflections.[46] Instead, the second-order spot (02) along the *c* direction at 16.1 Å and the higher-order spot (11) along the *a* direction are highlighted with red circles to illustrate the lattice indexing. The lattice parameters are consistent at both locations. However, the diffraction from the region marked by the green box in Figure 3B shows more higher-order reflections along both the *a* and *c* directions. Conversely, fewer higher-order spots are observed in the diffraction from the region within the blue box in Figure 3C. It suggests the different crystallinity at these areas.

Similarly, a HAADF-STEM micrograph of a $FNpe_5Nmepe$ crystal is shown in Figure 3D, with regions indicated by colored boxes 3 and 4. Electron diffraction patterns from these areas (Figure 3E,F) reveal similar unit cell dimensions. The first-order diffraction spots (01) at 32.4 Å and (10) at 4.5 Å are not visible,

https://doi.org/10.1021/acs.nanolett.5c02506
Nano Lett. 2025, 25, 11940−11946

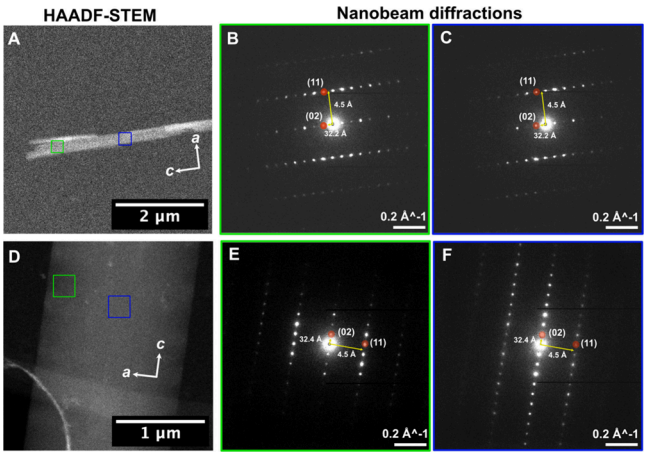

Figure 3. Local heterogeneity in 3D crystals measured by 4D-STEM. (A) HAADF-STEM image obtained from the 3D crystal formed by $FNpe_6$. The crystal is bright. Two regions along the long axis of the crystal are indicated by the blue and green boxes, receptively. (B and C) Diffractions obtained in the area indicated by the green and blue boxes in part A. Two arrows indicate the lattice vectors at the first order along the *a* and *c* directions. The first-order spot (01) at 32.2 Å is invisible due to the forbidden symmetry of *Cm* plane symmetry. The second-order spot (02) at 16.2, the *c* spacing, is indicated by the red dot for the clarity of indexing. The first-order spot (10) along the *c* direction at 4.5 Å is not visible as well due to the symmetry. The higher-order spot (11) is indicated by the red dot. (D−F) Analogues of parts A−C, obtained from the 3D crystals formed by $FNpe_5Nmepe$. More diffractions obtained across crystals are shown in Figures S11 and S12.

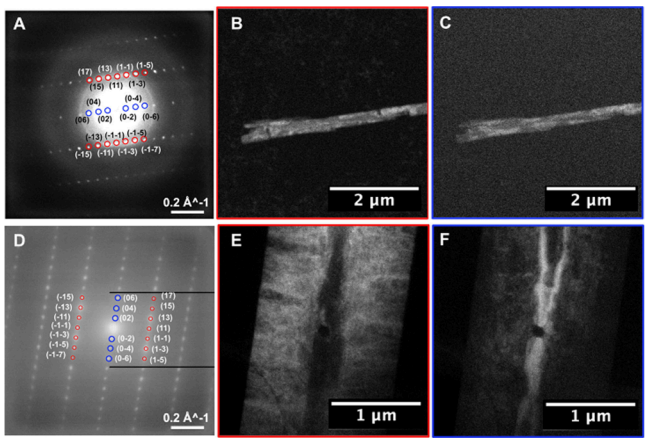

Figure 4. Virtual bright-field images of 3D crystals obtained by 4D-STEM. (A) Summed diffraction pattern obtained from the crystal formed by $FNpe_6$, which is shown in Figure 3A. Selected visible spots are indexed and indicated by red and blue circles along the *a* and *c* directions, respectively. (B and C) Virtual bright-field images obtained by reconstructing the information in the selected spots indicated by red and blue, respectively. The brighter regions represent the more ordered areas in the crystal. (D−F) Analogues of parts A−C, obtained from the 3D crystals formed by $FNpe_5Nmepe$.

due to the same symmetry constraints. However, the diffraction pattern from the area marked by the green box in Figure 3E exhibits notable higher-order reflections along the *a* direction but not the *c* direction. In contrast, the blue box region in Figure 3F shows more higher-order reflections along the *c* direction than the green box region. The absence of high-order spots along the *a* direction indicates less ordered molecular arrangement within rows. Conversely, the absence of high-order spots along the *c* direction suggests less ordered packing between rows. Additionally, it is noteworthy that the intensity of spots, which reflects the molecular arrangement along the *c* direction, such as (02), is more pronounced. This variation indicates that local heterogeneity in crystallinity varies between crystals formed by different oligopeptoids when comparing the diffractions.

To explore the origins of local heterogeneity in crystallinity, which is related to molecular arrangement in lattices, we generated virtual bright-field images. In these images, bright regions correspond to selected Bragg spots along the *a* and *c* directions, as observed in the summed electron diffraction patterns. Figure 4A shows a summed diffraction pattern that includes all patterns obtained from all probe positions in the 4D-STEM data set for the $FNpe_6$ crystal in Figure 3A. When the spots along the *a* direction, (1−5), (1−3), (11), (13), (15), (−1−5), (−1−3), (−11), (−13), and (−15), are selected, as indicated by red circles, the corresponding virtual bright-field image is shown in Figure 4B. Small, discontinuous bright areas are densely distributed across the crystal, indicating regions where molecules are well-ordered in rows. For the spots along the *c* direction, (0−6), (0−4), (0−2), (02), (04), and (06), selected as indicated by blue circles—the corresponding virtual bright-field image is shown in Figure 4C. Here, larger discontinuous bright areas are observed across the crystal. The presence of localized crystalline domains indicates that the molecules exhibit short-range orders along the *a* direction and relatively long-range orders along the *c* direction across the crystal. This observation is consistent with the similarities in the diffractions shown in Figures 3B and 3C, where two boxes were located at the end and center of the crystal, respectively. It suggests that that local heterogeneity in crystallization within a 3D crystal is due to short-range order packing in $FNpe_6$ crystals when the peptoid molecules have the unmodified *C*-terminus.

Figure 4D presents a summed diffraction pattern that includes all patterns obtained from all probe positions in the 4D-STEM data set for the $FNpe_5Nmepe$ crystal shown in Figure 3D, thereby making the high-order spots more evident. It is evident that $FNpe_5Nmepe$ crystals with the compact *C*-terminus exhibits more high-order spots, which indicate the long-range-ordered lattices compared to the results shown in Figure 4A. When spots along the *a* direction, (1−5), (1−3), (11), (13), (15), (−1−5), (−1−3), (−11), (−13), and (−15), are selected, as indicated by red circles in Figure 4C, the corresponding virtual bright-field image in Figure 4E shows that, in contrast, the center region is dark while bright regions are located at the edges of the crystal. This pattern indicates areas where molecules are well-ordered in rows, but the rows themselves are less ordered. Conversely, when the spots along the *c* direction, (0−6), (0−4), (0−2), (02), (04), and (06), were selected, as indicated by blue circles, the corresponding virtual bright-field image, shown in Figure 4F, shows that bright regions are located only in the center of the crystal, indicating well-ordered rows (refer to the unit cell model in Figure 1C). This observation aligns with the appearance of high-order spots in Figure 3E,F, where two boxes were positioned at the edge and center, respectively.

The XRD and electron microscopy imaging results indicate that the lattice spacings at (01) and (10) match those of 2D nanosheets formed by diblock peptoids of similar chemical compositions.[23] However, the *b* spacing along the vertical growth direction could not be directly measured due to the absence of ab initio reconstruction using microED. Our previous studies established a universal relationship between the molecular structure and crystal structure in diblock peptoids,

https://doi.org/10.1021/acs.nanolett.5c02506
Nano Lett. 2025, 25, 11940−11946

where the molecule length along the *b* direction is a linear function of the number of monomers (*N*) in the cis conformation, calculated as length (Å) = 2.9 Å × *N* ± 0.4 Å.[26] This model predicts the length of two monomers to be approximately 5.8 ± 0.4 Å. In $FNpe_6$ crystals, the first notable peak following the 16.05 Å (02) appears at 5.36 Å (06), a harmonic of the *c* spacing, while the absence of additional peaks near 5.8 Å suggests less ordering along the *b* direction. In contrast, the crystal formed by $FNpe_5Nmepe$ shows the new peak at 5.79 (close to the length of two monomers) in addition to the harmonic peak at 5.4 Å, along with the appearance of other peaks (5.16, 4.83, and 4.36 Å), which indicate enhanced crystallinity and molecular ordering along the *b* axis, consistent with higher melting temperature and enthalpy. Despite these variations, the fundamental motif of two monomers in a unit cell remains consistent, highlighting the capability to facilitate vertical growth from the previous 2D nanosheets to enable the hierarchical crystalline lattice design to afford 3D crystals with chemically modulable peptoids.

We propose a model for the unit cell and growth path of linear oligopeptoid 3D crystals, are stacked along the *b* direction in a head-to-tail configuration, as depicted in Figure 5. Figure 5A

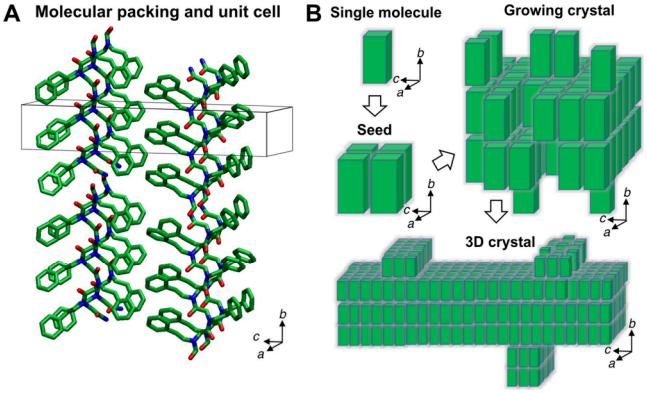

Figure 5. Schematics showing the molecular arrangement and formation pathway of 3D crystals. (A) Eight molecules arranged into two stacked rows along the *b* direction. The unit cell is shown as a black box in the top molecule. The 3D crystal formed by $FNpe_6$ has lattice dimensions of *a* = 4.51 Å, *b* = 5.80 Å (not directly measured), and *c* = 32.10 Å, whereas the crystal formed by $FNpe_5Nmepe$ features dimensions of *a* = 4.57 Å, *b* = 5.79 Å, and *c* = 32.40 Å. (B) Assembly pathway of 3D crystals from a single oligopeptoid molecule to 3D crystals indicating the hierarchical organization.

shows eight peptoid molecules with a unit cell highlighted in a blue box to represent the basic building block. The 3D crystal formed by $FNpe_6$ has lattice dimensions of *a* = 4.51 Å, *b* = 5.80 Å, and *c* = 32.10 Å, with a less ordered *b* direction, whereas the crystal formed by $FNpe_5Nmepe$ features dimensions of *a* = 4.57 Å, *b* = 5.79 Å, and *c* = 32.40 Å. The unit cell consists of a section of peptoid molecules. The simulated XRD profiles obtained from this model match major peaks in experimental profiles. (Figures S13)

The proposed crystallization pathway is depicted in Figure 5B, starting with a single molecule, which subsequently forms small crystals, composed of several molecules as seeds. More molecules stack along different directions to form 3D crystals. Athough the stacking order along the *b* direction appears the same in $FNpe_5Nmepe$ and $FNpe_6$ crystals because no obvious overlapping patterns or split spots are observed in small regions by 4D-STEM, AFM thickness measurements suggest that the growth along the *b* direction is more favored in $FNpe_5Nmepe$ crystals. The enhanced crystallinity and homogeneity of the 3D crystals with $FNpe_5Nmepe$ suggest that spatial occupation of the *C*-terminus plays a crucial role in the vertical growth. A similar end-group effect was confirmed in 3D crystals comprising $FNpe_5OPe$. This oligopeptoid features a phenylethyl ester moiety at the *C*-terminus. Compared to $FNpe_6$, $FNpe_5OPe$ formed thicker crystals (Figures S5 and S6) with higher crystallinity, as evidenced by XRD (Figure S7) and differential scanning calorimetry (DSC; Figure S8). These results highlight that end-group chemistry is crucial in controlling defects and promoting long-range order during the growth of 3D crystals from oligopeptoids.

This study investigates the formation of 3D crystals comprising linear oligomeric peptoids and how terminal modifications enhance crystallinity. Peptoids with a compact *C*-terminus formed thicker, more ordered crystals than those with an unmodified terminus, indicating the spatial effect of the terminus on modulating intermolecular contacts during crystallization. AFM imaging and 4D-STEM revealed significant deviations in the crystal thickness and inhomogeneities in the molecular arrangement, with some areas showing higher order along the *a* direction and others along the *c* direction. Lateral growth in the *a* and *c* directions is faster than growth in the *b* direction. We posit that the varying growth rates in different directions within different areas of the crystals are the primary source of the observed heterogeneity. The unit cell dimensions are characterized by a spacing of approximately 4.5 Å (*a* spacing) and 32.2 Å (*c* spacing), with the *b* spacing reflecting the distance of two monomers in the molecule in the cis conformation, which is not directly observable in $FNpe_6$ and approximately at 5.79 Å for $FNpe_5Nmepe$.

Remarkably, the 3D crystals in this study are formed by stacking molecules along the *b* direction, while retaining the similar unit cell dimensions (*a* and *c* directions) as that of the 2D peptoid crystals. This demonstrates that a linear hexapeptoid alone has a strong propensity to form a rectangular unit cell based on extended chains in a cis−Σ strand conformation, often seen in larger peptoid nanostructures. This study demonstrates the potential of hierarchical dimensional control to direct the 3D crystallization of oligomeric peptoids and paves the way for further research into the design and synthesis of complex soft materials with tailored properties.

■ ASSOCIATED CONTENT

Supporting Information

The Supporting Information is available free of charge at https://pubs.acs.org/doi/10.1021/acs.nanolett.5c02506.

Experimental section, which includes detailed materials characterization and structural analysis, for instance, the syntheses of peptoids, growth of 3D crystals, and techniques, including AFM, XRD, DSC, cryo-TEM, microED, and 4D-STEM imaging (Figures S1−S13 and Table S1) (PDF)

PDB file showing the peptoid molecules arrangement (PDB)

PDB file showing the unit cell (PDB)

■ AUTHOR INFORMATION

Corresponding Authors

Ronald N. Zuckermann − *Molecular Foundry, Lawrence Berkeley National Laboratory, Berkeley, California 94720,*

https://doi.org/10.1021/acs.nanolett.5c02506
Nano Lett. 2025, 25, 11940−11946

United States; orcid.org/0000-0002-3055-8860; Email: rnzuckermann@lbl.gov

Xi Jiang – *Materials Sciences Division, Lawrence Berkeley National Laboratory, Berkeley, California 94720, United States;* orcid.org/0000-0002-9589-7513; Email: xijiang@lbl.gov

Brooks A. Abel – *Materials Sciences Division, Lawrence Berkeley National Laboratory, Berkeley, California 94720, United States; Department of Chemistry, University of California, Berkeley, California 94720, United States;* orcid.org/0000-0002-2288-1975; Email: brooks.abel@berkeley.edu

Authors

Yen Jea Lee – *Materials Sciences Division, Lawrence Berkeley National Laboratory, Berkeley, California 94720, United States;* orcid.org/0000-0003-2699-8676

Peter Ercius – *Molecular Foundry, Lawrence Berkeley National Laboratory, Berkeley, California 94720, United States;* orcid.org/0000-0002-6762-9976

Xubo Luo – *Materials Sciences Division, Lawrence Berkeley National Laboratory, Berkeley, California 94720, United States;* orcid.org/0000-0002-1591-7466

Glenn L. Butterfoss – *Center for Genomics and Systems Biology, New York University, New York, New York 10003, United States*

Tianyi Yu – *Materials Sciences Division, Lawrence Berkeley National Laboratory, Berkeley, California 94720, United States*

Jian Zhang – *Molecular Foundry, Lawrence Berkeley National Laboratory, Berkeley, California 94720, United States;* orcid.org/0000-0003-0274-0814

David Prendergast – *Molecular Foundry, Lawrence Berkeley National Laboratory, Berkeley, California 94720, United States;* orcid.org/0000-0003-0598-1453

Andrew M. Minor – *Molecular Foundry, Lawrence Berkeley National Laboratory, Berkeley, California 94720, United States; Department of Materials Science and Engineering, University of California, Berkeley, California 94720, United States;* orcid.org/0000-0003-3606-8309

Nitash P. Balsara – *Materials Sciences Division, Lawrence Berkeley National Laboratory, Berkeley, California 94720, United States; Department of Chemical and Biomolecular Engineering, University of California, Berkeley, California 94720, United States;* orcid.org/0000-0002-0106-5565

Complete contact information is available at: https://pubs.acs.org/10.1021/acs.nanolett.5c02506

Author Contributions

Y.J.L. synthesized materials, prepared 3D crystals, and carried out characterizations and 4D-STEM measurements. P.E. and A.M.M. assisted with 4D-STEM measurements and data analysis. X.L., D.P., and G.B. contributed to the modeling. T.Y. synthesized the materials that inspired this work. J.Z. assisted with XRD measurements. N.P.B., R.N.Z., B.A.A., and X.J. designed experiments. R.N.Z., B.A.A., and X.J. supervised this work. X.J. performed cryo-TEM imaging and microED. The funding for this work was led by N.P.B.. Y.J.L. and X.J. wrote the manuscript. All authors contributed to reviewing and finalizing the manuscript.

Notes

The authors declare no competing financial interest.

■ ACKNOWLEDGMENTS

Primary funding for this work was provided by the Soft Matter Electron Microscopy Program (KC11BN), supported by the Office of Science, Office of Basic Energy Science, U.S. Department of Energy, under Contract DE-AC02-05CH11231. Work at the Molecular Foundry at Lawrence Berkeley National Laboratory was supported by user projects at these user facilities, supported by the Office of Science, Office of Basic Energy Sciences, U.S. Department of Energy, under Contract DE-AC02-05CH11231. This research used resources of the National Energy Research Scientific Computing Center (NERSC), a Department of Energy Office of Science User Facility using NERSC award BES-ERCAP0032327. Micrographs presented here were obtained at the Berkeley Bay Area Cryo-EM facility (BACEM) at the University of California, Berkeley. We thank George Meigs and James Holton for their assistance with the XRD measurements, and Natalia Molchanova and Michael Connolly for their help with peptoid synthesis.

■ REFERENCES

(1) Desiraju, G. R. Supramolecular Synthons in Crystal Engineering - a New Organic-Synthesis. *Angew. Chem. Int. Edit* **1995**, *34* (21), 2311–2327.

(2) Moulton, B.; Zaworotko, M. J. From molecules to crystal engineering: Supramolecular isomerism and polymorphism in network solids. *Chem. Rev.* **2001**, *101* (6), 1629–1658.

(3) Vargo, E.; Ma, L.; Li, H.; Zhang, Q. T.; Kwon, J.; Evans, K. M.; Tang, X. C.; Tovmasyan, V. L.; Jan, J.; Arias, A. C.; et al. Functional composites by programming entropy-driven nanosheet growth. *Nature* **2023**, *623* (7988), 724–731.

(4) Hakobyan, K.; Noble, B. B.; Xu, J. T. The current science of sequence-defined macromolecules. *Prog. Polym. Sci.* **2023**, *147*, 101754.

(5) Li, Z.; Wang, S. Z.; Nattermann, U.; Bera, A. K.; Borst, A. J.; Yaman, M. Y.; Bick, M. J.; Yang, E. C.; Sheffler, W.; Lee, B.; et al. Accurate computational design of three-dimensional protein crystals. *Nat. Mater.* **2023**, *22* (12), 1556–1563.

(6) Cui, H. G.; Krikorian, V.; Thompson, J.; Nowak, A. P.; Deming, T. J.; Pochan, D. J. Preparation and characterization of synthetic polypeptide single crystals with controlled thickness. *Macromolecules* **2005**, *38* (17), 7371–7377.

(7) Yuan, C. Q.; Ji, W.; Xing, R. R.; Li, J. B.; Gazit, E.; Yan, X. H. Hierarchically oriented organization in supramolecular peptide crystals. *Nature Reviews Chemistry* **2019**, *3* (10), 567–588.

(8) Datta, S.; Grant, D. J. W. Crystal structures of drugs: Advances in determination, prediction and engineering. *Nat. Rev. Drug Discov* **2004**, *3* (1), 42–57.

(9) Steigerwald, M. L.; Brus, L. E. Semiconductor Crystallites - a Class of Large Molecules. *Acc. Chem. Res.* **1990**, *23* (6), 183–188.

(10) de la Rica, R.; Matsui, H. Applications of peptide and protein-based materials in bionanotechnology. *Chem. Soc. Rev.* **2010**, *39* (9), 3499–3509.

(11) Price, S. L. Predicting crystal structures of organic compounds. *Chem. Soc. Rev.* **2014**, *43* (7), 2098–2111.

(12) Schmidt, T.; Bergner, A.; Schwede, T. Modelling three-dimensional protein structures for applications in drug design. *Drug Discov Today* **2014**, *19* (7), 890–897.

(13) Margolin, A. L.; Navia, M. A. Protein crystals as novel catalytic materials. *Angew. Chem., Int. Ed.* **2001**, *40* (12), 2204–2222.

(14) Sontz, P. A.; Bailey, J. B.; Ahn, S.; Tezcan, F. A. A Metal Organic Framework with Spherical Protein Nodes: Rational Chemical Design of 3D Protein Crystals. *J. Am. Chem. Soc.* **2015**, *137* (36), 11598–11601.

(15) Zhou, K.; Zang, J. C.; Chen, H.; Wang, W. M.; Wang, H. F.; Zhao, G. H. On-Axis Alignment of Protein Nanocage Assemblies from 2D to 3D through the Aromatic Stacking Interactions of Amino Acid Residues. *ACS Nano* **2018**, *12* (11), 11323–11332.

(16) Zhang, S.; Alberstein, R. G.; De Yoreo, J. J.; Tezcan, F. A. Assembly of a patchy protein into variable 2D lattices via tunable multiscale interactions. *Nat. Commun.* **2020**, *11* (1), 3770.
(17) Burattini, S.; Greenland, B. W.; Merino, D. H.; Weng, W. G.; Seppala, J.; Colquhoun, H. M.; Hayes, W.; Mackay, M. E.; Hamley, I. W.; Rowan, S. J. A Healable Supramolecular Polymer Blend Based on Aromatic π-π Stacking and Hydrogen Bonding Interactions (vol 132, pg 12051, 2010). *J. Am. Chem. Soc.* **2021**, *143* (26), 10016−10017.
(18) Vijayakanth, T.; Dasgupta, S.; Ganatra, P.; Rencus-Lazar, S.; Desai, A. V.; Nandi, S.; Jain, R.; Bera, S.; Nguyen, A. I.; Gazit, E.; et al. Peptide hydrogen-bonded organic frameworks. *Chem. Soc. Rev.* **2024**, *53* (8), 3640−3655.
(19) Hu, X. Z.; Liao, M. R.; Gong, H. N.; Zhang, L.; Cox, H.; Waigh, T. A.; Lu, J. R. Recent advances in short peptide self-assembly: from rational design to novel applications. *Curr. Opin. Colloid Interface Sci.* **2020**, *45*, 1−13.
(20) Ide, Y.; Manabe, Y.; Inaba, Y.; Kinoshita, Y.; Pirillo, J.; Hijikata, Y.; Yoneda, T.; Shivakumar, K.; Tanaka, S.; Asakawa, H.; et al. Determination of the critical chain length for macromolecular crystallization using structurally flexible polyketones. *Chemical Science* **2022**, *13* (34), 9848−9854.
(21) Kirshenbaum, K.; Barron, A. E.; Goldsmith, R. A.; Armand, P.; Bradley, E. K.; Truong, K. T. V.; Dill, K. A.; Cohen, F. E.; Zuckermann, R. N. Sequence-specific polypeptoids: A diverse family of heteropolymers with stable secondary structure. *Proc. Natl. Acad. Sci. U.S.A.* **1998**, *95* (8), 4303−4308.
(22) Jin, H.; Ding, Y.-H.; Wang, M.; Song, Y.; Liao, Z.; Newcomb, C. J.; Wu, X.; Tang, X.-Q.; Li, Z.; Lin, Y.; et al. Designable and dynamic single-walled stiff nanotubes assembled from sequence-defined peptoids. *Nat. Commun.* **2018**, *9* (1), 270.
(23) Xuan, S. T.; Jiang, X.; Spencer, R. K.; Li, N. K.; Prendergast, D.; Balsara, N. P.; Zuckermann, R. N. Atomic-level engineering and imaging of polypeptoid crystal lattices. *Proc. Natl. Acad. Sci. U.S.A.* **2019**, *116* (45), 22491−22499.
(24) Yu, T. Y.; Luo, X. B.; Prendergast, D.; Butterfoss, G. L.; Rad, B.; Balsara, N. P.; Zuckermann, R. N.; Jiang, X. Structural Elucidation of a Polypeptoid Chain in a Crystalline Lattice Reveals Key Morphology-Directing Role of the N-Terminus. *ACS Nano* **2023**, *17* (5), 4958−4970.
(25) Eastwood, J. R. B.; Weisberg, E. I.; Katz, D.; Zuckermann, R. N.; Kirshenbaum, K. Guidelines for designing peptoid structures: Insights from the Peptoid Data Bank. *Peptide Sci.* **2023**, *115* (3). DOI: 10.1002/pep2.24307.
(26) Greer, D. R.; Stolberg, M. A.; Kundu, J.; Spencer, R. K.; Pascal, T.; Prendergast, D.; Balsara, N. P.; Zuckermann, R. N. Universal Relationship between Molecular Structure and Crystal Structure in Peptoid Polymers and Prevalence of the &ITcis&IT Backbone Conformation. *J. Am. Chem. Soc.* **2018**, *140* (2), 827−833.
(27) Jiang, N. S.; Yu, T. Y.; Darvish, O. A.; Qian, S.; Tsengam, I. K. M.; John, V.; Zhang, D. H. Crystallization-Driven Self-Assembly of Coil-Comb-Shaped Polypeptoid Block Copolymers: Solution Morphology and Self-Assembly Pathways. *Macromolecules* **2019**, *52* (22), 8867−8877.
(28) Jiao, F.; Wu, X. P.; Jian, T. Y.; Zhang, S.; Jin, H. B.; He, P. G.; Chen, C. L.; De Yoreo, J. J. Hierarchical Assembly of Peptoid-Based Cylindrical Micelles Exhibiting Efficient Resonance Energy Transfer in Aqueous Solution. *Angew. Chem., Int. Ed.* **2019**, *58* (35), 12223−12230.
(29) Sun, J.; Wang, Z. W.; Zhu, C. H.; Wang, M. Y.; Shi, Z. K.; Wei, Y. H.; Fu, X. H.; Chen, X. S.; Zuckermann, R. N. Hierarchical supramolecular assembly of a single peptoid polymer into a planar nanobrush with two distinct molecular packing motifs. *Proc. Natl. Acad. Sci. U.S.A.* **2020**, *117* (50), 31639−31647.
(30) Li, Z. L.; Cai, B.; Yang, W. C.; Chen, C. L. Hierarchical Nanomaterials Assembled from Peptoids and Other Sequence-Defined Synthetic Polymers. *Chem. Rev.* **2021**, *121* (22), 14031−14087.
(31) Song, S. F.; Xu, J. T.; Zhou, H.; Manners, I.; Winnik, M. A. Focal Point Association of Core-Crystalline Micelles with an Amphiphilic Corona Block. *J. Am. Chem. Soc.* **2025**, *147* (11), 9919−9930.
(32) Jiang, X.; Seidler, M.; Butterfoss, G. L.; Luo, X. B.; Yu, T. Y.; Xuan, S. T.; Prendergast, D.; Zuckermann, R. N.; Balsara, N. P. Atomic-Scale Corrugations in Crystalline Polypeptoid Nanosheets Revealed by Three-Dimensional Cryogenic Electron Microscopy. *ACS Macro Lett.* **2023**, *12* (5), 632−638.
(33) Nam, K. T.; Shelby, S. A.; Choi, P. H.; Marciel, A. B.; Chen, R.; Tan, L.; Chu, T. K.; Mesch, R. A.; Lee, B. C.; Connolly, M. D.; et al. Free-floating ultrathin two-dimensional crystals from sequence-specific peptoid polymers. *Nat. Mater.* **2010**, *9* (5), 454−460.
(34) Sun, J.; Teran, A. A.; Liao, X. X.; Balsara, N. P.; Zuckermann, R. N. Crystallization in Sequence-Defined Peptoid Diblock Copolymers Induced by Microphase Separation. *J. Am. Chem. Soc.* **2014**, *136* (5), 2070−2077.
(35) Mannige, R. V.; Haxton, T. K.; Proulx, C.; Robertson, E. J.; Battigelli, A.; Butterfoss, G. L.; Zuckermann, R. N.; Whitelam, S. Peptoid nanosheets exhibit a new secondary-structure motif. *Nature* **2015**, *526* (7573), 415−420.
(36) Jin, H.; Ding, Y. H.; Wang, M.; Song, Y.; Liao, Z.; Newcomb, C. J.; Wu, X.; Tang, X. Q.; Li, Z.; Lin, Y.; et al. Designable and dynamic single-walled stiff nanotubes assembled from sequence-defined peptoids. *Nat. Commun.* **2018**, *9* (1), 270.
(37) Hammons, J. A.; Baer, M. D.; Jian, T. Y.; Lee, J. R. I.; Weiss, T. M.; De Yoreo, J. J.; Noy, A.; Chen, C. L.; Van Buuren, A. Early-Stage Aggregation and Crystalline Interactions of Peptoid Nanomembranes. *J. Phys. Chem. Lett.* **2021**, *12* (26), 6126−6133.
(38) Zhao, M.; Lachowski, K. J.; Zhang, S.; Alamdari, S.; Sampath, J.; Mu, P.; Mundy, C. J.; Pfaendtner, J.; De Yoreo, J. J.; Chen, C.-L.; et al. Hierarchical Self-Assembly Pathways of Peptoid Helices and Sheets. *Biomacromolecules* **2022**, *23* (3), 992−1008.
(39) Xuan, S.; Jiang, X.; Spencer, R. K.; Li, N. K.; Prendergast, D.; Balsara, N. P.; Zuckermann, R. N. Atomic-level engineering and imaging of polypeptoid crystal lattices. *Proc. Natl. Acad. Sci. U. S. A.* **2019**, *116* (45), 22491−22499.
(40) Martynowycz, M. W.; Gonen, T. From electron crystallography of 2D crystals to MicroED of 3D crystals. *Curr. Opin. Colloid Interface Sci.* **2018**, *34*, 9−16.
(41) Ophus, C. Four-Dimensional Scanning Transmission Electron Microscopy (4D-STEM): From Scanning Nanodiffraction to Ptychography and Beyond. *Microscopy and Microanalysis* **2019**, *25* (3), 563−582.
(42) Bustillo, K. C.; Zeltmann, S. E.; Chen, M.; Donohue, J.; Ciston, J.; Ophus, C.; Minor, A. M. 4D-STEM of Beam-Sensitive Materials. *Acc. Chem. Res.* **2021**, *54* (11), 2543−2551.
(43) Chen, M.; Bustillo, K. C.; Patel, V.; Savitzky, B. H.; Sternlicht, H.; Maslyn, J. A.; Loo, W. S.; Ciston, J.; Ophus, C.; Jiang, X.; et al. Direct Imaging of the Crystalline Domains and Their Orientation in the PS--PEO Block Copolymer with 4D-STEM. *Macromolecules* **2024**, *57* (12), 5629−5638.
(44) Kanomi, S.; Marubayashi, H.; Miyata, T.; Tsuda, K.; Jinnai, H. Nanodiffraction Imaging of Polymer Crystals. *Macromolecules* **2021**, *54* (13), 6028−6037.
(45) Panova, O.; Chen, X. C.; Bustillo, K. C.; Ophus, C.; Bhatt, M. P.; Balsara, N.; Minor, A. M. Orientation mapping of semicrystalline polymers using scanning electron nanobeam diffraction. *Micron* **2016**, *88*, 30−36.
(46) Dorset, D. L. *Structural Electron Crystallography*; Plenum Press, 1995.